# 3D Wavelet Analysis of Computed Tomography Images in Pneumatic Conveying

**M. Takei[1] H.Li[2] M.Ochi[1] Y.Saito[3] and K.Horii[4]**

1. Department of Mechanical Engineering,Nihon University
   1-8-14 KandaSurugadai Tokyo 101-8308 Japan
2. Kagoshima University, Kagoshima Japan
3. Hosei Univ., Tokyo Japan        4. Shirayuri College, Tokyo Japan

**Abstract** – Particle flow CT images at the upstream of a bend pipe is decomposed to the time levels to extract dominant particle density distribution using three-dimensional discrete wavelets transform. As a result, the high density of the particle spatial distribution at the front of a dense flow, which composes high time frequency level, is located at the upper part than that just over the stationary layer. It reveals that the particles composing the plug at the front are steep and are discharged toward the front air phase.

**Keywords:** Capacitance CT, 3D Wavelets, Solid-Air Two Phase Flow, Image Processing

## 1. INTRODUCTION

Dense flow in a pipeline has been typically used in various industries such as a chemical, a pharmaceutical, and a food industries. The basic physical properties of the dense flow should be measured in order to provide the predictive mechanism for the pipeline design. The particle movement of the dense plug flow is visualized by a high-speed camera (Klinzing G.E, 2001); it reveals qualitatively the particle flow within the plug from the pickup at the beginning to the falling off at the end. Moreover, quantitatively, velocities of particles composing a plug front end was measured at cross-sectional grids in a pipeline by means of LDV to discuss the movement patterns of the particles (Takei,M et al. 1998). However, the LDV method cannot measure the entire cross section; therefore, it is difficult to understand the three-dimensional particle movement in a dense flow. Under these circumstances, capacitance CT together with real time visualization has been studied as a technique by which to visualize particle behavior in a cross section of a pipeline (Dyakowski,T. et al. 1999). This capacitance CT arranges a sensor consisting of many electrodes around the circumference of a pipeline in order to measure the capacitances between the electrodes. The distribution of particle density based on the permittivity distribution on the cross section is obtained via a reconstruction method. However, the images obtained by the capacitance CT are blurred because the approximate values are resolved using a mathematical ill-posed inverse problem. Image analysis is necessary in order to extract the features of the blurred images in order to ascertain the dominant particles from the image.

Currently, in mechanical engineering fields, wavelets transform is being performed using image analysis rather than Fourier transform. The merits of wavelets analysis is the ability to analyze the frequency, while not removing time information. The discrete wavelets transform has been used primarily for picture image processing. The orthonormal transform of this analysis enables quantitative decomposition and recomposition of a picture image. A number of researchers applied this idea to the analysis of a jet image (Li,H, et al.,1999). Generally, two-dimensional wavelets transform has been used to obtain the two dimensional original image.

The originality of the present method lies in the application of three-dimensional discrete wavelets transform to a three-dimensional capacitance CT image in order to extract the particle pattern features in a particle dense flow at the upstream of a bend pipe. In the present study, particle capacitances upstream of a pipe bend are measured to re-construct the particle density images using two-dimensional space and time. The images are transformed by three-dimensional discrete wavelets in order to extract the dominant time particle levels.

## 2. EXPERIMENTS

The equipment for the present experiment consisted of a feeder tank, a pipeline of 49.0 mm inside diameter, a receiver tank and a Root's blower, as shown in Fig. 1. A CT sensor having 12 electrodes was arranged around the pipe circumference upstream of the pipe bend. The air suction volume was 0.019 $m^3$/s, and the particle was supplied at 390.0 g/s. The mean air velocity in the pipeline as calculated from the air volume was 9.10 m/s. The Reynolds number was $2.92 \times 10^4$. The solid air ratio was 12.46. The particles were polyethylene pellets, which were almost spherical, having a 3.26-mm diameter and a density of 910 kg/$m^3$. The time interval necessary to acquire one frame is $\Delta t = 10.0$ ms. The 512 consecutive frames for 5,120.0 ms are selected from among the total reconstructed frames obtained for 60.0 seconds for analysis in the next section. In the present study, the permittivity matrix, which indicates the particle two-dimensional space distribution at a time, is normalized via a calibration using the maximum value of 1.0 and the minimum value of 0.0. The maximum value indicates the situation whereby the particles occupy the entire cross-section. The minimum value indicates the situation whereby the air occupies the entire cross-section. One image pixel is $1.53 \times 1.53$ mm$^2$. The inside cross-section 49.0 mm is divided by $32 \times 32$ image pixels. When a particle core passes through the measurement section, the diameter of one particle takes up 2.13 image pixels because the particle diameter is 3.26 mm.

The reconstructed three-dimensional image obtained by the CT is re-calculated to obtain the density image by dividing by the root mean square value. The representative particle density images from $50\Delta t$ to $400\Delta t$ at $50\Delta t$ step ($\Delta t = 10$ ms) are shown in Fig. 2. The image pixel, at which no particle exists, is blue. As the particle density on an image pixel becomes high, the image pixel turns red as shown in the color bar. At the upstream of a bend pipe, particles in the dense flow are accumulated resulting in the plug flow. As a reference, Fig. 3 shows the side view of the plug. From Figs. 2 and 3, on the whole, the time transient distributions of the particle density are qualitatively visualized. In order to confirm roughly the particle movement during the time, the spatial mean particle density at a time are calculated to show in Fig.4. This figure reveals that five dense flows passed through the pipe cross section during the time (denote 1,2 3,4 and 5), and three dense flows 1,2 and 3 plug the pipe cross section entirely. In the next section, the highly dense flow 1, 2 and 3 are analyzed by three dimensional wavelet multiresolutions.
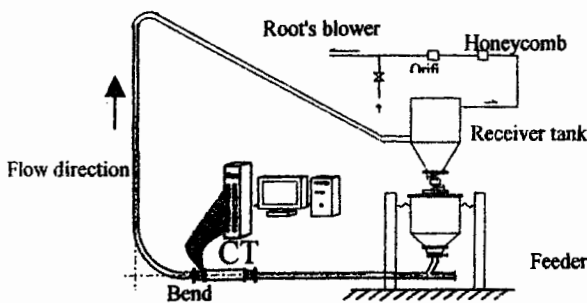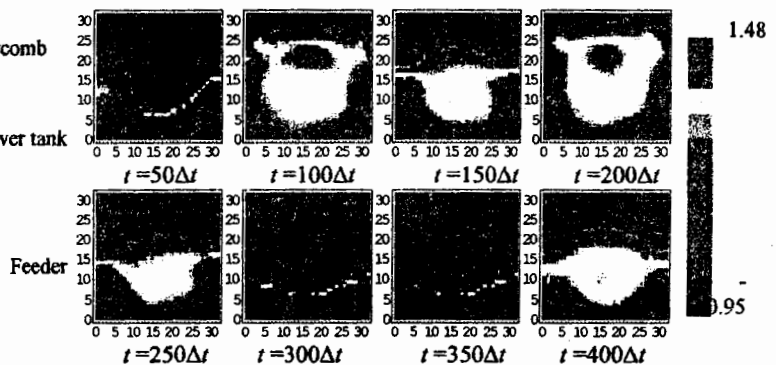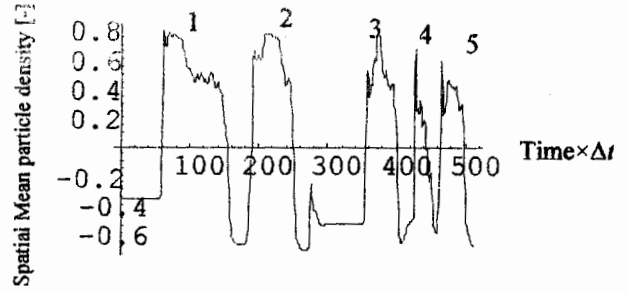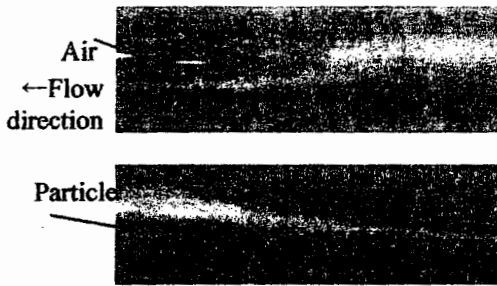


**Fig. 1 Experimental equipment.**



**Fig. 2 Representative Images.**

Fig. 3 Side view of plug.



Fig. 4 Spatial mean particle density.

# 3. ANALYSIS AND DISCUSSION

## 3.1. 3D Discrete Wavelets Transform

The three-dimensional wavelets spectrum $S_{tyx}$ is obtained by

$$S_{tyx} = [W_t[W_y[W_x E_{xyt}]^T]^T]^T \qquad (1)$$

where, $E_{xyt}$ is a three-dimensional original image consisting of $Nx \times Ny \times Nt$ pixels. $Nx$, $Ny$ and $Nt$ are pixels in the $x$, $y$ (space axis) and $t$ (time axis) dimensions, respectively, $W_x$, $W_y$ and $W_t$ are the analyzing wavelet matrices consisting of $Nx \times Nx$ pixels, $Ny \times Ny$ pixels and $Nt \times Nt$ pixels, respectively. The transpose matrices are defined as

$$[E_{xyt}]^T = E_{txy} \quad [E_{txy}]^T = E_{ytx} \quad [E_{ytx}]^T = E_{xyt} \qquad (2)$$

Therefore, the wavelets spectrum $S_{tyx}$ is composed of $Nt \times Ny \times Nx$ pixels. The inverse three dimensional wavelets transform of Eq. (1) is expressed as

$$E_{xyt} = [W_x[W_y[W_t S_{tyx}]^T]^T]^T \qquad (3)$$

For $2^{nd}$-order Daubechies orthonormal functions of the analyzing wavelets, and original image data consisting of $Nx=Ny=32$, $Nt=512$, an original image can be decomposed to each frequency the level as shown in Fig.5, namely,

$$E_{xyt} = E_0 + E_1 + E_2 + E_3 + E_4 + E_5 + E_6 + E_7 + E_8 + E_9 \qquad (4)$$

$$E_0 = [W_x[W_y[W_t S_0]^T]^T]^T E_1 = [W_x[W_y[W_t S_1]^T]^T]^T \ldots E_8 = [W_x[W_y[W_t S_8]^T]^T]^T \ E_9 = [W_x[W_y[W_t S_9]^T]^T]^T$$

where, $S_0$ is the lowest frequency spectrum, and $S_5$ is the highest frequency spectrum. Therefore, $E_0$, the image inversely transformed from $S_0$, indicates the particle two-dimensional space distribution having the lowest time frequency, which is referred to as time level 0. Thus, time level 0 indicates the time mean space distribution. On the other hand, $E_9$, the image inversely transformed from $S_9$, indicates the two-dimensional space distribution having the highest time frequency, which is referred to as time level 9. Time level 9 therefore indicates the most time-fluctuated space distribution. Fig.6 shows the power spectrum of the analyzing wavelet of Daubechies function of $2^{nd}$ order.



Fig.5 Multiresolution by 3D wavelets.



Fig.6 Power spectrum of analyzing wavelet.

15.10
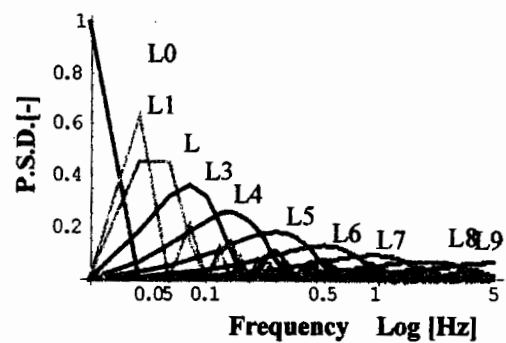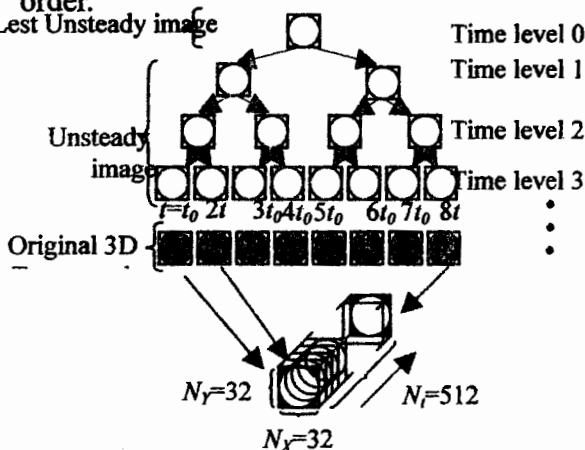
## 3.2 Multiresolution Images

The three-dimensional original images of the particle density in Fig.2 are decomposed by three dimensional wavelet multiresolution of Eq.(4). The values outside the pipe wall are replaced with the lowest value to clarify the images. The lowest time frequency of the time level 0 indicates the steady two-dimensional space distribution of the particle density during the time. The highest time frequency of the time level 9 indicates the least steady distribution of the particle density. Fig. 7 shows the example of the decomposed images from the original image at $100\Delta t$, which is the middle part of the dense flow 1 according to Fig. 4. The color map values are different among the original, the level 0 and the more than the level 1 images. The summation of all level images at each space element completely recovers the original image in Fig. 2 due to the orthonormal wavelets transform. From Fig. 7, the lowest frequency level 0 indicates the time-mean particle density spatial distribution; namely, the distribution is mainly a stationary layer, which is located at the pipeline bottom. Also, the figure 7 reveals that the relative low frequency level 3 dominates the particle movement at $100\Delta t$ among these levels, and the spatial particle distribution in the level 3 is located above the stationary layer of the time-mean location in the level 0. Moreover, in the levels 1 and 2, both sides above the stationary layer have slight yellow parts (denote A), indicating the particle density is changed at these parts with low frequency. And then, yellow parts are slightly visible at the upper part of the cross section in the levels 6 and 7 (denote B). It means particles densities at the upper part are changed slightly with high frequency. In order to confirm dominant levels of the total particle movement, the spatial-mean values of the particle density images decomposed by the wavelets multiresolution are calculated. Figure 8 is the results from the level 3 to the level 7. Some levels are omitted because the levels do not clearly appear a peak. In the level 3, three high values to denote 1, 2 and 3 are visible at the period from $65\Delta t$ to $128\Delta t$, from $193\Delta t$ to $250\Delta t$, and from $354\Delta t$ to $384\Delta t$, which are equivalent to the numbers in Fig. 4. The particle density of each level at the start and end times of those periods are visualized to discuss the particle movement in detail. First, the period 1 is discussed. Just before the start time; at $64\Delta t$, in the levels 6 and 7, a high value is appeared (denote 1-s), which indicates the front of the start time. At the end time of the period 1; $132\Delta t$, in the levels 4 and 5, a high value is appeared (denote 1-e). As the time goes, at $148\Delta t$ in the levels 6 and 7, a high value is appears, and the high value moves to $156\Delta t$ in the level 7 (denote 1-e). Next, the period 2 is discussed. At $192\Delta t$ in the levels 6 and 7, a high value is appeared (denote 2-s). At the end time of the period 2; $240\Delta t$, the high value is slightly appeared (denote 2-e) in the level 5. As the time goes, at $243\Delta t$ in the level 6 (denote 2-e), a high value is appeared, and the high value moves to $250\Delta t$ in the level 7 (denote 2-e). Finally, the period 3 is discussed. From $354\Delta t$ in the level 4, a high value is appeared (denote 3-s), the period is included in the period 3 in the level 3. Therefore, at the period 3, the level 4 is dominant rather than the level 3 in terms of the low frequency. At the start time near $354\Delta t$, the high level such as the levels 6 and 7 do not a high value. At the end time; $384\Delta t$ in the level 5 (denote 3-e), a high value is appeared. As the time goes, the high value moves to $400\Delta t$ in the level 6, $402\Delta t$ in the level 7 (denote 3-e). The above discussion reveals that at the start time of each period, a high value is appeared in the higher level; the high value moves to higher level as the time passes.

Next, the start and end times of the first period are focused to confirm the flow pattern in detail. Figure 9 is the decomposed images of the front and rear of the dense flow at the period 1 as a representative image. The periods 2 and 3. shows the similar images. The horizontal axis is the time and the vertical axis is the wavelet levels. The color bar is the same as that in Fig. 7. At $64\Delta t$ in Fig.9, indicating the front of the dense flow, values in high level of the levels 6 and 7 are high; however, values in high levels of the levels 3, 4 and 5 are nearly zero. It means high time frequency particles compose the front of the dense flow. Moreover, the particle spatial distribution is located at the upper part of the stationary layer in the high frequency. Precisely, in the level 6, the high value is located at the upper part (denote C) than that just over the stationary layer (denote D). From $65\Delta t$ to $128\Delta t$ when the main body passes, the low level 3 is dominant. At $132\Delta t$, indicating the rear of the dense flow, high particle density is shown in the levels 4 and 5; however, the particle density is low in the levels 5 and 6. As the time goes to $148\Delta t$, the high density is shown in level 6 and 7; however,

the particle density is low in the level 5. Moreover, at $156\Delta t$, the high density is shown in only level 7, and then, the high density is disappeared at $157\Delta t$. With regard to the spatial distribution, at $132\Delta t$, a high-density part is located at the top in the level 5; then, the high-density part moves to the middle in the level 6 at $148\Delta t$; and then, the high-density part moves to the bottom in the level 7 at $156\Delta t$. Namely, as the time passes, the dominant level moves from the level 5 to the level 7, and the dominant spatial parts move from the top to the bottom. From the abovementioned discussion it is clarified that the front of the dense flow is steep, whose part passes through the cross section at high time-period indicating the level 6 and 7; on the other hand, the rear is gently slope, indicating gradually change from the level 4 to the level 7. Figure 10 is measurement results of particle velocity at a front consisting of a dense flow by means of Laser Doppler Velocimeter (Takei,M, et al.,1998). The horizontal axis is velocity rate $V_p/V_s$. The vertical axis is the high rate $y/D$ ($D$ is the pipe diameter). $Vp$ is the particle velocity at the front by LDV. $V_s$ is the main plug velocity, which is obtained from two residual images of time retardation photograph. $U$ is the air velocity. (A),(B),(C) and (D) show the velocities at $x/D$=0.5(center point),$x/D$=0.63, $x/D$=0.76 and $x/D$=0.90(near wall), respectively. The $x$ and $y$ axes are shown in Fig.4(c). In Fig.10 (A), the particle velocity is higher than the plug main velocity at the center of the dense flow; however, as the measurement point gets close to the near wall, the particle velocity gets lower than the plug main velocity, irrespective of the air velocity. It reveals that the particles composing the dense flow at the front are discharged toward the front air phase as shown in Fig. 11. This tendency indicates that the decomposed levels 6 and 7 images at $64\Delta t$ in Fig.9 are the reasonable particle distributions.
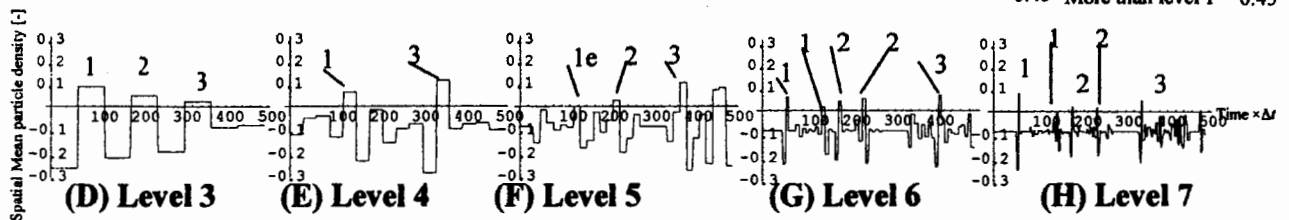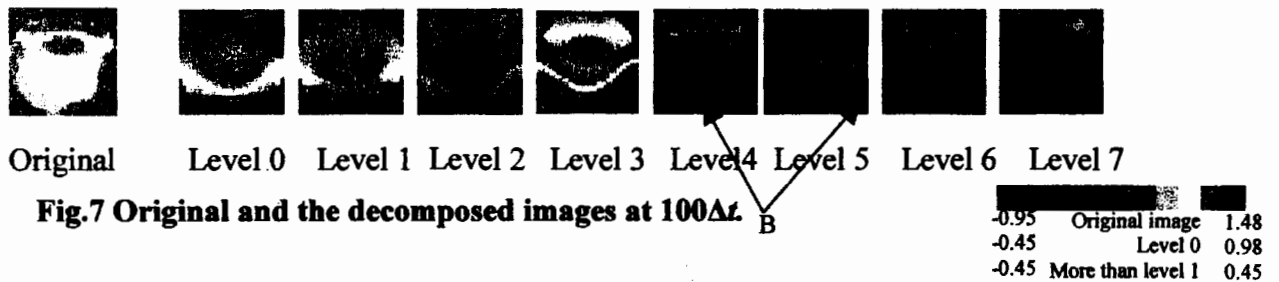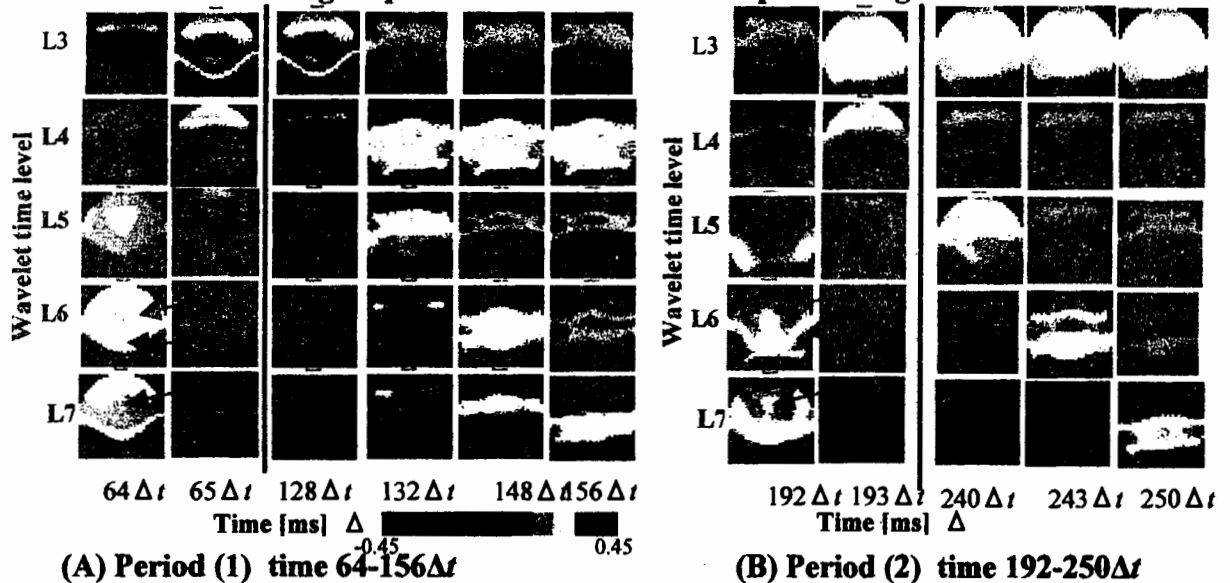


Original    Level 0    Level 1   Level 2   Level 3   Level 4   Level 5    Level 6    Level 7

**Fig.7 Original and the decomposed images at $100\Delta t$.**

|  | | |
|---|---|---|
| -0.95 | Original image | 1.48 |
| -0.45 | Level 0 | 0.98 |
| -0.45 | More than level 1 | 0.45 |



**(D) Level 3        (E) Level 4        (F) Level 5            (G) Level 6            (H) Level 7**

**Fig.8 Spatial mean value of decomposed images.**



64$\Delta t$   65$\Delta t$   128$\Delta t$   132$\Delta t$   148$\Delta t$156$\Delta t$        192$\Delta t$ 193$\Delta t$ 240$\Delta t$   243$\Delta t$ 250$\Delta t$

Time [ms]  $\Delta$                                                Time [ms]  $\Delta$

**(A) Period (1)  time 64-156$\Delta t$**                              **(B) Period (2)  time 192-250$\Delta t$**

**Fig.9 Front and rear of dense flow.**

(A) x/R=0.0          (B) x/R=0.79                                    (B) Near pipe wall
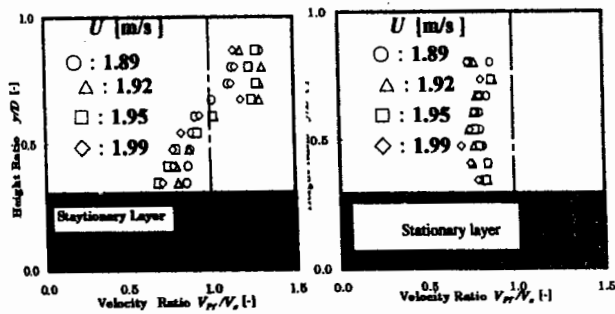
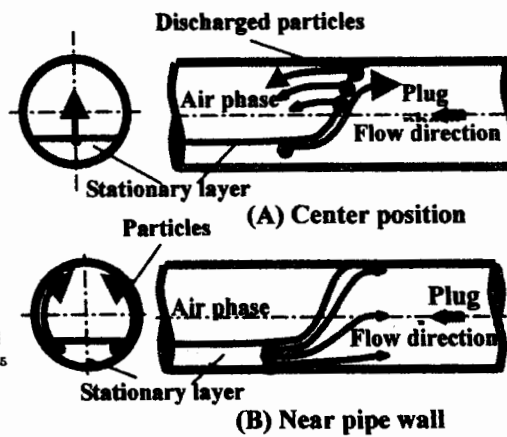**Fig.10 Particle velocities by LDV.**          **Fig.11 Particle movement model at front part.**

## 4. CONCLUSIONS

The dominant time levels of a dense flow on a pipeline cross section was performed using capacitance-computed tomography and three-dimensional wavelets transform to analyze the particle density of the dense flow at a bend upstream. The following findings were obtained.

(1) The formation of the particle density at the front of a dense flow composes the levels 6 and 7, which indicates the high time frequency level. The high density of the particle spatial distribution is located at the upper part than that just over the stationary layer. It makes sure that the particles composing the dense flow at the front are steeper than the rear.

(2) The particle density at the rear of the dense flow moves from the level 5 to the level 7; moreover, the dominant spatial part moves from the top to the bottom as the time passes. It indicates the dense flow formation, whose rear is gently slope.

(3) The comparison between CT image and LDV measurement reveals that the particles composing the dense flow at the front are discharged toward the front air phase; moreover, it is possible to visualize the discharging particles distribution in detail.

## 5. REFERENCES

Dyakowski,T., Luke,S.P., Ostrowski,K.L. and Williams,R.A. (1999) On-Line Monitoring of Dense Phase Flow Using Real Time Dielectric Imaging, *Powder technol*, 104, pp.287-295.

Klinzing G.E, (2001) Dense Phase (plug) Conveying –Observations and Projections--, *Handbook of Conveying and Handling of Particulate Solids*, Edited by A.Levy, and H.Kalman, Elsevier Science B.V., pp329-341

Li,H., Takei, M., et al. (1999) Application of Two-dimensional Orthogonal Wavelets to Multiresolution Image Analysis of a Turbulent Jet, *Transactions of the Japan Society for Aeronautical and Space Sciences*, Vol.42, No.137, pp.120-127.

Takei,M, Ochi,M. et al. (1998) Movement of Particles Composing Plug at Front End, *Transactions of the Japan Society of Mechanical Engineers*, Vol64, No.628, pp.86-92 (in Japanese)

## 6. ACKNOWLEDGEMENT